J Neurophysiol
87: 15–29, 2002; 10.1152/jn.00394.2001.

Giant Miniature EPSCs at the Hippocampal Mossy Fiber to CA3 Pyramidal Cell Synapse Are Monoquantal

DARRELL A. HENZE,[1] DAVID B. T. MCMAHON,[1] KRISTEN M. HARRIS,[2] AND GERMAN BARRIONUEVO[1]
[1]*Department of Neuroscience and Center for the Neural Basis of Cognition, University of Pittsburgh, Pittsburgh, Pennsylvania 15260; and* [2]*Program in Neuroscience and Department of Biology, Boston University, Boston, Massachusetts 02215*

Received 16 May 2001; accepted in final form 2 October 2001

Henze, Darrell A., David B. T. McMahon, Kristen M. Harris, and German Barrionuevo. Giant miniature EPSCs at the hippocampal mossy fiber to CA3 pyramidal cell synapse are monoquantal. *J Neurophysiol* 87: 15–29, 2002; 10.1152/jn.00394.2001. The mechanisms generating giant miniature excitatory postsynaptic currents (mEPSCs) were investigated at the hippocampal mossy fiber (MF) to CA3 pyramidal cell synapse in vitro. These giant mEPSCs have peak amplitudes as large as 1,700 pA (13.6 nS) with a mean maximal mEPSC amplitude of 366 ± 20 pA (mean ± SD; 5 nS; $n = 25$ cells). This is compared with maximal mEPSC amplitudes of <100 pA typically observed at other cortical synapses. We tested the hypothesis that giant mEPSCs are due to synchronized release of multiple vesicles across the release sites of single MF boutons by directly inducing vesicular release using secretagogues. If giant mEPSCs result from simultaneous multivesicular release, then secretagogues should increase the frequency of small mEPSCs selectively. We found that hypertonic sucrose and spermine increased the frequency of both small and giant mEPSCs. The peptide toxin secretagogues alpha-latrotoxin and pardaxin failed to increase the frequency of giant mEPSCs, but the possible lack of tissue penetration of the toxins make these results equivocal. Because a multiquantal release mechanism is likely to be mediated by a spontaneous increase in presynaptic calcium concentration, a monoquantal mechanism is further supported by results that giant mEPSCs were not affected by manipulations of extracellular or intracellular calcium concentrations. In addition, reducing the temperature of the bath to 15°C failed to desynchronize the rising phases of giant mEPSCs. Together these data suggest that the giant mEPSCs are generated via a monovesicular mechanism. Three-dimensional analysis through serial electron microscopy of the MF boutons revealed large clear vesicles (50 to 160 nm diam) docked presynaptically at the MF synapse in sufficient numbers to account for the amplitude and frequency of giant mEPSCs recorded electrophysiologically. It is concluded that release of the contents of a single large clear vesicle generates giant mEPSCs at the MF to CA3 pyramidal cell synapse.

INTRODUCTION

The mossy fiber (MF) synapse between granule cells of the dentate gyrus and the pyramidal cells of hippocampal area CA3 has many unique anatomical, electrophysiological and pharmacological properties (see Henze et al. 2000 for review). For example, in a previous study, we demonstrated that the mean MF miniature excitatory postsynaptic current (mEPSC) peak amplitude is twice as large as the peak of non-MF mEPSCs (24.6 vs. 12.2 pA, respectively) (Henze et. 1997). In addition, we have observed that the peak conductance of individual MF mEPSCs can be up to two orders of magnitude larger (>10 nS) than the peak conductance of mEPSCs generally attributed to "conventional," i.e., non-MF synapses onto cortical pyramidal cells (<750 pS) (Bekkers et al. 1990; Bolshakov and Siegelbaum 1995; Henze et al. 1997; Hestrin 1992; Manabe et al. 1992; Raastad et al. 1992; Wyllie et al. 1994). We called these large MF mEPSCs "maxi" or giant mEPSCs and proposed that they might be generated by a mechanism distinct from that underlying the generation of non-MF mEPSCs.

Several pre- or postsynaptic mechanisms for the generation of giant MF mEPSCs have been considered. Possible presynaptic mechanisms include increased vesicular glutamate concentration, increased vesicle size, and/or synchronized multivesicular release. Possible postsynaptic mechanisms include differential electrotonic filtering of the MF synaptic currents, increased density or number of AMPA receptors, and/or large conductance AMPA receptors lacking the GluR-B subunit. Most of these potential mechanisms cannot easily explain a 100-fold range in mEPSC amplitude at the MF synapse. Therefore we hypothesized (Henze et al. 1997) that the giant mEPSCs arise due to calcium-dependent synchronized multivesicular release across the multiple release sites known to occur between a single MF giant bouton and an individual CA3 pyramidal cell (Amaral and Dent 1981; Hamlyn 1962). Evidence for multivesicular release has been recently demonstrated at cerebellar inhibitory synapses (Llano et al. 2000). At the MF bouton, multivesicular release across multiple release sites could account for both the large amount of released glutamate and the large number of postsynaptic AMPA receptors that would be needed to generate a mEPSC with a peak conductance >10 nS. Here we investigate whether the giant mEPSCs have a mono- or multivesicular origin by applying secretagogues, manipulating presynaptic calcium concentrations, and changing temperature. We also use serial electron microscopy to determine whether there are large enough clear vesicles in sufficient numbers to account for the giant mEPSCs. Our results suggest that MF giant mEPSCs are due to monove-

Present address and address for reprint requests: D. A. Henze, Center for Molecular and Behavioral Neuroscience, Rutgers, The State University of New Jersey, 197 University Ave., Newark, NJ 07102 (E-mail: Henze @axon.rutgers.edu).

The costs of publication of this article were defrayed in part by the payment of page charges. The article must therefore be hereby marked "*advertisement*" in accordance with 18 U.S.C. Section 1734 solely to indicate this fact.

sicular release of glutamate from extraordinarily large synaptic vesicles (more than ~60 nm diam) that dock in the same locations as small vesicles. We further propose that the glutamate released from these giant vesicles diffuses to multiple postsynaptic densities within a single MF synaptic complex.

METHODS

Tissue slices for in vitro electrophysiology were prepared from Sprague-Dawley rats 27 to 40 days old (Hilltop Labs, Hilltop, PA). Animals were deeply anesthetized with equithesin (10.88 g chloral hydrate, 5.44 g $MgSO_4 \cdot 7\ H_2O$, and 2.5 g pentobarbitol dissolved in 25.6 ml 95% ethanol, 65 ml isopropylene glycol, and water to a final volume of 256.4 ml), and their chest cavities were rapidly opened. The rats were then transcardially perfused with a cold oxygenated solution with the following composition (in mM): 229 sucrose, 1.9 KCl, 1.2 Na_2PO_4, 25 $NaHCO_3$, 10 glucose, and 6.0 $MgCl_2$ (Aghajanian and Rasmussen 1989). Prior to the transcardial perfusion, the sucrose solution was bubbled with 97.5% O_2-2.5% CO_2 to adjust the pH to 7.4 at 4°C. The hippocampus was rapidly removed and transverse slices (350–500 μm) were prepared using a vibratome.

Following sectioning, slices were maintained at room temperature (19–23°C) in an artificial cerebrospinal fluid (ACSF) consisting of (in mM) 126 NaCl, 3.5 KCl, 1.2 Na_2PO_4, 11 glucose, 25 $NaHCO_3$, 3.0 $MgCl_2$, and 3.0 $CaCl_2$. The ACSF was bubbled with 95% O_2-5% CO_2 (pH to 7.4). For recording, individual slices were transferred as needed (between 2 and 12 h following slice preparation) to a submerged chamber where they were superfused with oxygenated ACSF at 33°C.

Electrophysiological recordings

Spontaneous mEPSCs were recorded using the "blind" whole cell recording technique (Blanton et al. 1989) and a voltage-clamp amplifier (PC-501or PC 505, Warner Instruments, Hamden, CT). Current-clamp recordings were performed with a Axoclamp 2B amplifier (Axon Instruments, Foster City, CA). All voltage-clamp recordings were done with the membrane potential clamped at −80 mV unless otherwise specified. Recordings were filtered at 2–5 kHz using the Bessel filters of the amplifier. Continuous recordings of each experiment were collected simultaneously to a chart recorder as well as digitized at 22 kHz for storage on video tape using a Neuro-corder (NeuroData Instruments). At the end of each experiment, 3-min epochs were replayed from the VCR tapes and digitized at 10 kHz and stored on computer hard disk for subsequent analysis. The 3-min epochs were selected for having a stable baseline and stable series resistance. Whole cell pipettes were filled with one of two solutions each with a pH of 7.3 and osmolarity of 305–330 mOsm: *1*) 122.5 cesium gluconate, 17.5 CsCl, 10 HEPES, 0.2 EGTA, 8 NaCl, 2 $MgCl_2$, 4 MgATP, 0.3 NaGTP, and 10 Na phosphocreatine, referred to as CsGluc solution. And *2*) 100 potassium gluconate, 20 KCl, 10 HEPES, 0.2 EGTA, 4 MgATP, 0.3 NaGTP, and 10 Na phosphocreatine, referred to as KGluc solution.

The majority of the experiments used CsGluc with a few experiments using KGluc as indicated in the text. Unexpectedly, the KGluc solution resulted in a generalized increase in mEPSC frequency across all amplitudes. However, no differences were observed in the qualitative outcome of the experiments, and so the KGluc cases have been included. No corrections for junction potentials were made.

In all cases, filled pipettes had a resistance of 3–6 MΩ in the bath. Most recordings had series resistances <10 MΩ. During some recordings, series resistance increased, and series resistance compensation was utilized to maintain a constant effective series resistance. During recording, data were rejected if the uncompensated series resistance became >20 MΩ or if compensation caused large changes in the baseline noise. All recordings were carried out in the presence of 1 μM tetrodotoxin (TTX; Sigma) and 10 μM bicuculline methiodide (Sigma) to block action potentials and $GABA_A$-mediated inhibitory postsynaptic currents (IPSCs), respectively. All drugs were delivered by bath application except for hypertonic sucrose (see RESULTS). All salts, tetrodotoxin, bicuculline, probenecid, and caffeine were obtained from Sigma (St. Louis, MO). Alpha Latrotoxin and pardaxin were obtained from Alomone Labs (Jerusalem, Israel). BAPTA-AM was obtained from Molecular Probes (Eugene, OR). Cyclopiazonic acid, thapsigargin, and 2-hydroxypropyl-γ-cyclodextrin were obtained from RBI (Natick, MA).

Automated mEPSC detection algorithm

The detection and measurement of the mEPSCs was accomplished using an automated routine based on the derivatives of the recorded waveform. The algorithm is similar to previously published automated detection algorithms for detecting mEPSCs and mIPSPs (Ankri et al. 1994; Henze et al. 1997; Malgoroli and Tsien 1992). The detection algorithm was executed in the LabView programming environment (National Instruments, Austin, TX) and run on a Pentium-based PC. Following the initial automated detection and measurement, each file was examined by hand to delete the events associated with the series resistance test pulses as well as any spurious noise transients. It was determined that the algorithm often generated false positive errors for most events measuring <10 pA, so all events <10 pA were ignored. Finally, in some cases where the mEPSCs overlapped closely in time or the mEPSC rising phase was long enough to have noise, there were two peaks in the first derivative without an intervening zero crossing. In this case, the algorithm yielded an output of identical two mEPSCs occurring at the same point in time. The second entry of these "double detections" were deleted from the data sets.

Electrophysiological analysis and statistics

Three ranges of mEPSC peak amplitudes were selected for statistical examination. The ranges chosen were 20–30, 50–60, and >100 pA. These ranges were chosen for two reasons. First, mEPSCs were observed in sufficient numbers in each amplitude range. It would not have been possible to select a range from 100 to 110 pA because many recordings failed to display more than one or two mEPSCs in this range. The second reason for choosing these ranges was based on previous data (Henze et al. 1997) where we showed that although a large proportion of mEPSCs at 20–30 pA are from non-MF synapses (~50%), the MFs give rise to >95% of the mEPSCs at 50–60 and all mEPSCs >100 pA.

Changes in the frequencies of mEPSCs at the three selected peak amplitude ranges, as well as the overall mEPSC frequency, were tested statistically in one of two ways. If the experimental design was such that each cell served as its own control, then the experimental frequencies were expressed as percent of control and tested as a group against a normal distribution centered at 100% using Student's *t*-tests. On the other hand, if the experimental design precluded within cell comparisons, then the nonparametric Mann Whitney-*U* test was used to compared the raw numbers of mEPSCs detected in control and experimental recordings for each peak amplitude range. All mean values are given as ±SE.

Quantification of inflections in the rising phase of giant mEPSCs

The following method was used to quantify the asynchrony of the rising phases of mEPSCs as a function of temperature. A metric was developed based on the assumption that if an mEPSC is due to the release of a single quantized pulse of neurotransmitter, the mEPSC is expected to have a shape with smooth rising and decaying phases that are well approximated by an alpha function and/or the sum of two squared exponential functions. Similar functions have been shown to

describe synaptic EPSCs in a number of preparations (Bekkers and Stevens 1996; Brown and Johnston 1983; Hestrin et al. 1990; Williams and Johnston 1991). If an mEPSC is not fit by such a function, then its kinetics are influenced by factors other than a simple monovesicular pulsatile release of neurotransmitter. For example, the rising phases of the waveforms are expected to have inflected rising phases if mEPSCs are due to slightly asynchronous release of multiple vesicles. The magnitude and number of these inflections are expected to increase as the temperature is decreased due to a slowing of the reactions that underlie the release of individual vesicles (e.g., Katz and Miledi 1965).

The following protocol was used to measure inflections in the rising phase of giant mEPSCs.

mEPSCs >100 pA were extracted from 3-min epochs recorded at a variety of temperatures from 16 to 33°C. Temperatures below the ambient room temperature of ~20°C were accomplished by perfusing the water jacket of the recording chamber with ice-cold water. Temperature above room temperature were accomplished using the heating element permanently mounted inside the recording chamber water jacket.

Each giant mEPSC was then fit with the following equation: If $(x - X_o) < 0$, then

$$y = Y_o + B_m * x$$

(a straight line).

If $(x - X_o) > 0$, then

$$y = (R_{mag} * (1 - \exp(-x - X_o/R_t))^2) + (D_{mag} * (1 - \exp(-x - X_o/D_t))^2) + (B_m * x) + Y_o$$

(the sum of 2 squared exponentials summed with a line), where x = time; y = amplitude; X_o = offset in time from the beginning of the trace; Y_o = offset of the recording baseline from zero; B_m = baseline slope, R_{mag} = rising phase magnitude, R_t = rising tau, D_{mag} = decay phase magnitude; and D_t = decay phase tau.

Note: The straight line portion of the fitting equation is to account for slow variations in the baseline over the time course of the mEPSC.

A numerical estimate of the deviation of the waveform from the expected kinetics was determined using the sum of the squared residuals (SSR) over the rising phase (baseline to negative peak) of the mEPSC and the 2 ms of baseline preceding the waveform, divided by the number of points over that time. This indicator was chosen because the output values should be large when mEPSC rising phases are inflected and "asynchronous" and small when the mEPSC rising phases are smooth and "synchronous." Figure 3*A* shows the result of using the equation above to fit two individual giant mEPSCs, one obviously inflected and one smooth. The "residual" waveforms over the rising-phase after subtracting the fit from the raw data are shown also.

Determination of a threshold for rising phase inflection

It also was necessary to determine a threshold value for the mEPSC rising phase SSRs which, when exceeded, indicated an inflection was present and not just a normal amount of error due to fitting biologically noisy data. The normal amount of biological noise was determined by fitting realistic noisy waveforms known to be smooth. The method described in the following text accounts for the two possible sources of noise. First, the method determines the average SSR value given the noise intrinsic to electrophysiological recording in these recording conditions. Second, the method determines if background "undetected" small mEPSCs can spontaneously overlap with rising phases of large, and often slow, mEPSCs and cause inflections or apparent asynchrony.

The threshold criterion for an inflected waveform was determined separately for each recording as follows: *1*) "noisy" smooth waveforms (NSWs) were generated by adding the best-fit waveforms output from the fitting of the real data with periods between mEPSCs from the same recordings. *2*) The NSWs were then subjected to the same fit analysis as the "real" data (see preceding text). *3*) The mEPSC rising phase SSR for the NSWs were then compared with the SSRs for the original real data waveforms. *4*) The threshold criterion for "inflection" for each separate recording epoch was defined as the mean SSR for the NSW fits plus two times the standard deviation of the NSW fit SSRs.

If the SSRs for the fit of any real waveform exceeds the established threshold for that recording, then there is some additional factor influencing the kinetics of the rising phases of large mEPSCs besides simple receptor kinetics and electrotonic filtering. The extra influence cannot be due to spontaneous overlap of small, undetected, background mEPSCs because the noise traces used to determine the threshold for rising phase inflections were taken from the same data sets as the original large mEPSCs. If small undetected mEPSCs accounted for all of the detected inflections, then the NSWs should have the same amount of inflections as the original data. Inflections in the mEPSC rising phase cannot be due to the activation of postsynaptic voltage-gated active conductances due to the recording conditions (TTX, intracellular cesium, and voltage clamp at −80 mV).

Tissue preparation and electron microscopy

New serial EM sections were obtained from hippocampal area CA3 from a young adult male rat of the Long-Evans strain (310 g, ~70 days old). Perfusion and tissue processing were done as previously described (Chicurel and Harris 1992; Harris and Stevens 1989). Briefly, perfusion through the heart was performed under deep pentobarbital anesthesia with 2% paraformaldehyde and 2.5% glutaraldehyde in 0.1 M cacodylate buffer with 2 mM $CaCl_2$, pH 7.4. The hippocampus was removed and sectioned into 400-mm-thick slices. These slices were rinsed in buffer and then soaked in 1% OsO_4 with 1.5% $K_4Fe(CN)_6$ for 1 h followed by immersion in OsO_4 for an additional hour. The slices were then rinsed in buffer, soaked for 5 min each in 30 and 50% ethanol, immersed for 1 h in 1% uranyl acetate in 70% ethanol, dehydrated through graded ethanols and propylene oxide, and embedded in Epon. Blocks were trimmed to contain the hippocampal CA3 pyramidal cell bodies and their apical dendrites in stratum lucidum. Serial sections were cut on a Reichert Ultracut E ultramicrotome, mounted on Pioloform-coated slot grids (Synaptek) and stained for 5 min with Reynolds' lead citrate.

Each grid was put into a grid cassette, mounted on a modified rotating stage (JEOL SRH-10 Mod) to obtain consistent orientation of adjacent sections, and photographed at a JEOL 1200EX electron microscope. Three samples located ~30 μm from the CA3 pyramidal cell layer in stratum lucidum were photographed at ×10,000 magnification through 78 serial sections. Section thickness was determined as previously described by measuring the diameter of longitudinally sectioned mitochondria and then counting the number of serial sections the mitochondria traversed (section thickness = mitochondrial diameter/No. of sections). The mean section thickness determined by measuring 12 mitochondria was 0.055 μm. Thus small vesicles identified as having a continuous membrane appeared on just one section.

Active zone selection and vesicle analysis

Forty-five complete active zones (AZs) were identified within the series. Six mossy fiber boutons each contained one or more complete AZs including: 26, 3, 6, 4, 1, 4 for a total of 44 AZs. AZs were selected for further analysis if they were unobscured and the postsynaptic density (PSD) was cut perpendicular to the plane of the section throughout the series. This criterion made it possible to measure the distance of synaptic vesicles from the release site within a single micrograph. Eleven AZs were identified based on these criteria and analyzed under higher magnification using the image analysis software IGLtrace (http://synapses.bu.edu).

Three pools of synaptic vesicles were delineated within each presynaptic varicosity including the proximal nondocked pool, docked vesicles, and a distal pool. The proximal pool was defined by the region within 100 nm of the presynaptic release site delineated by the three-dimensional extent of the PSD. Within the proximal pool, docked vesicles were identified by their direct apposition to the presynaptic membrane at the release site (Harris and Sultan 1995). The proximal pool of vesicles was outlined to create a region of interest which was then moved back to capture a distal pool of vesicles of equal volume and shape and located between 250 and 350 nm from the release site. In 3 of the 11 AZs, the diameters of vesicles could not be measured in the distal pool because the presynaptic varicosities were too small, and the region of interest extended beyond the boundaries of the presynaptic varicosity. Population histograms (Fig. 7) were constructed on the basis of vesicle diameters measured from the distal, proximal nondocked, and docked vesicle pools. In total, 1,466 distal, 1,215 proximal nondocked vesicles, and 185 docked vesicles were measured.

All animal experimental protocols were approved by the animal care and use committees at the respective institution where the work was done.

RESULTS

Spontaneous mEPSCs recorded from the soma of CA3 pyramidal cells arise from excitatory synapses made by other ipsi- and contralateral CA3 pyramidal cells as well as from the MF synapse made by granule cells of the ipsilateral dentate gyrus. The mean maximal mEPSC peak amplitude from CA3 pyramidal cells is 366 ± 20 pA (±SD; 5 nS; $n = 25$ cells), and there are some cases where the maximal mEPSC peak amplitude is well over 1.0 nA (13 nS; Fig. 1*A*). These giant mEPSCs recorded from CA3 pyramidal cells are removed by a γ-irradiation-induced lesion of the granule cells that give rise to the MFs (Henze et al. 1997), indicating that they are of MF origin.

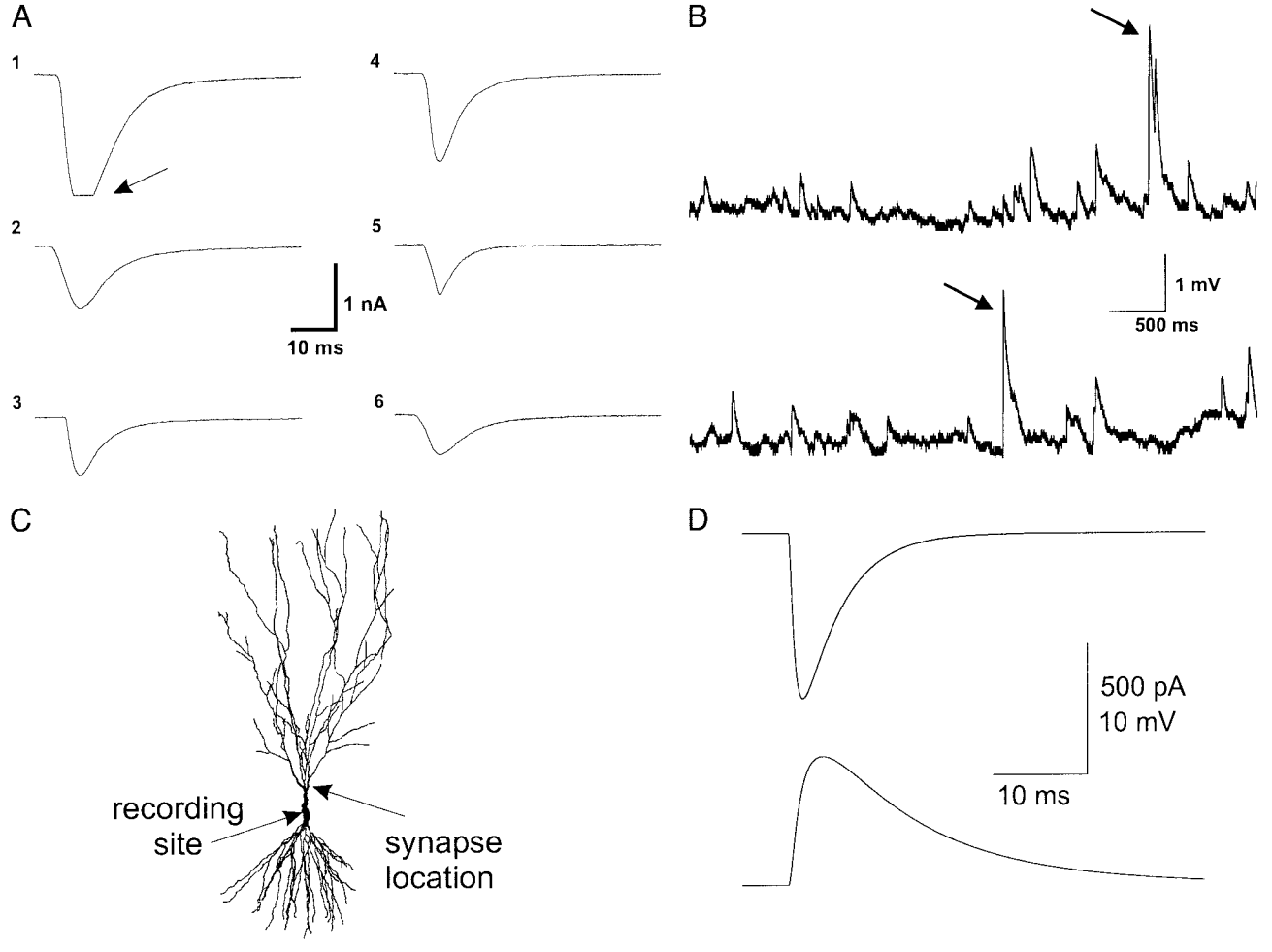

FIG. 1. Examples of very large miniature excitatory postsynaptic currents (mEPSCs) recorded from CA3 pyramidal cells. *A*: each waveform represents a single isolated mEPSC recorded from a CA3 pyramidal cell under voltage-clamp conditions with a holding potential of −80 mV. The flat peak of waveform 1 was caused by the extremely large peak current that causes saturation of the output stage of the amplifier at 1,749 pA. The peak amplitudes of the other waveforms are 906 pA (2), 837 pA (3), 1280 pA (4), 722 pA (5), and 561 pA (6). *B*: examples of large excitatory postsynaptic potentials (EPSPs) recorded from a CA3 pyramidal cell. Two 5-s epochs of spontaneous mEPSPs recorded under current-clamp conditions from a CA3 pyramidal cell resting at −68 mV. Notice the 2 synaptic events that exceed 2 mV in amplitude (←). *C* and *D*: simulation of the depolarization of a CA3 pyramidal cell due to a mEPSC with a large peak conductance (400-pA peak amplitude from a 8.5-nS peak conductance). *C*: drawing of the simulated cell with the locations of the "synaptic" and "recording" sites indicated. *D, top*: a simulated EPSC recorded at −80 mV holding potential with a simulated access resistance of 8 MΩ (similar to what was used for empirical data collection). *Bottom*: the same simulated synaptic event as in *C* recorded in current clamp at a resting potential of −60 mV. Notice that it is ~10 mV in amplitude.

The giant mEPSCs are of particular interest because they will contribute significantly to cellular depolarization and excitability. Figure 1*B* shows a current clamp recording from a CA3 pyramidal cell in the standard conditions of TTX and bicuculline. This cell was resting at approximately −68 mV and several examples of ~3 mV depolarizations due to mEPSPs can be seen, consistent with a previous report of large CA3 mEPSPs (Brown et al. 1979). Furthermore, when a giant MF mEPSC is generated (400 pA peak amplitude) in a compartmental simulation of a CA3 pyramidal neuron (see Henze et al. 1996 for details of simulation), it results in a 10-mV depolarization at the soma (Fig. 1, *C* and *D*).

We operationally defined the largest mEPSCs as "giant" if they had peak amplitudes >100 pA (1.25 nS) based on the following factors. First, mEPSCs of this size are never seen in recordings from cells in slices without MF synapses (Henze et al. 1997; Urban et al. 2001). Similarly, an mEPSC of 100 pA is twice as large as the largest mEPSCs attributed to the non-MF synapses (Henze et al. 1997). This criterion ensures that the selected giant mEPSCs are not mixed with non-MF mEPSCs. Finally, a 100 pA (1.25 nS) mEPSC is ~10 times larger than the reported quantal peak amplitude for the MF synapse (133 pS) (Jonas et al. 1993). If the quantum of neurotransmission in the MFs has a Gaussian distribution with a mean of 133 pS and a coefficient of variation of 22% (Jonas et al. 1993), then monoquantal mEPSCs 10 times larger than the modal peak amplitude are predicted to be so rare statistically that they may never be observed. Our goal was to determine whether or not there is a mechanistic rationale to make a distinction between mEPSCs with large and small peak amplitudes.

Are giant mEPSCs due to synchronous multivesicular release?

There is evidence that a spontaneous multivesicular mechanism can cause large mEPSCs at synapses with multiple release sites (Korn et al. 1993, 1994). This multivesicular mechanism may be a mechanism for the giant MF mEPSCs because the MF synapse has multiple synaptic release sites between an individual giant synaptic bouton and a single CA3 pyramidal cell (Amaral and Dent 1981; Hamlyn 1962). In addition, Jonas et al. (1993) reported that the mean quantal size for the MF synapse is 133 pS while we have seen an mEPSC as large as 21 nS (see Fig. 1).

Hypertonic sucrose increases the frequency of mEPSCs of all sizes

The proposed synchronous multivesicular mechanism for the generation of giant mEPSCs requires a signal that synchronizes the release of the multiple vesicles across the multiple release sites of the MF bouton. If vesicular release is induced downstream of a synchronizing signal, then the frequency of giant mEPSCs due to synchronized multivesicular release will decrease relative to the frequency of smaller monovesicular mEPSCs. One treatment that has been shown to induce direct vesicular release is the application of hypertonic sucrose solutions. Due to difficulties in maintaining stable recordings during prolonged bath application of hypertonic solutions, hypertonic sucrose (100 mM sucrose in regular ACSF) was applied for a few minutes at a time from a large bore pipette placed above the *stratum lucidum* of the slice in the area of the recording pipette. The sucrose solution was gravity fed to the surface of the slice for several minutes then the pipette was withdrawn. Prolonged hypertonic sucrose application tended to "rundown" the mEPSC frequency so 1-min recording epochs were used for this analysis.

Figure 2*A* shows the effect of 100 mM hypertonic sucrose solution on mEPSC frequency. The application of the hypertonic solution rapidly increased the frequency of all mEPSCs, regardless of peak amplitude (548 ± 174%; Student's 1-tailed *t*-test, $P = 0.0224$; $n = 5$). Similar to the overall effect of hypertonic treatment, the frequency of giant mEPSCs was also increased (589 ± 296%), although this effect failed to be significant statistically (Student's 1-tailed *t*-test, $P = 0.0694$; $n = 5$). Although in every case sucrose increased the frequency of the giant mEPSCs, the lack of statistical significance on the giant mEPSCs is due to the large variance in the percent changes because the smallest increase was 277% while the largest percent change was 1635%. These experiments were done with the KGluc pipette solution. Similar results were obtained in two additional recordings using CsGluc electrodes (data not shown). If these two additional cells are included in the analysis, the standard error is reduced and the relative increase in frequency of giant mEPSCs is significant (508 ± 191%; Student's 1-tailed *t*-test, $P = 0.0381$; $n = 7$).

It is concluded that hypertonic bathing media increased the frequency of mEPSCs at all peak amplitudes. These data suggest that the mechanism by which hypertonic sucrose induces mEPSC release is the same for all mEPSCs regardless of their size and are inconsistent with the hypothesis of a synchronous multivesicular release underlying giant mEPSCs.

Secretagogues α-latrotoxin and pardaxin increase the frequency of small mEPSCs

Two toxins, α-latrotoxin (α-LTX) (Capogna et al. 1996; see Petrenko 1993 for review) and pardaxin (PDX) (Lazarovici and Lelkes 1992) have been shown to induce direct vesicular release via both calcium-dependent and independent mechanisms. Figure 2*B* illustrates the effect of a 20- to 30-min application of 1 nM α-latrotoxin on CA3 mEPSC frequency. Five to 10 min after the change to bath solution containing the α-LTX, a sudden increase in mEPSC frequency was observed. It can be seen that α-LTX increased the mean overall frequency of observed mEPSCs (353 ± 1129%, Student's 1-tailed *t*-test, $P = 0.0395$; $n = 6$). It also can be seen that despite the large increase in the overall frequency of mEPSCs, there was not an increase in the frequency of giant mEPSCs. In fact, giant mEPSC frequency actually decreased (62 ± 20%, Student's 1-tailed *t*-test, $P = 0.0469$; $n = 6$).

Figure 2*C* shows the effect of a 15- to 30-min application of 1–2 μM PDX. Similar to the effect of α-LTX, PDX also increased the mean overall mEPSC frequency (667 ± 262%; Student's 1-tailed *t*-test, $P = 0.0215$; $n = 5$). The effect of PDX also had similar onset to that of α-LTX in that 5–10 min after the change to bath solution containing the PDX, a sudden increase in mEPSC frequency was observed. Like α-LTX, PDX produced a large increase in the frequency of the smallest amplitude mEPSCs. Notice however, that there was some increase in the frequency of medium and large size events as

reflected in the binned analysis (Fig. 2*C, bottom*). The frequency of giant mEPSCs was increased by 223 ± 75%, although this effect was not significant (Student's 1-tailed *t*-test, $P = 0.113$; $n = 5$).

In general, these observations could be consistent with the synchronous multivesicular hypothesis. However, PDX increased the frequency of giant mEPSCs to a lesser extent than the small mEPSCs. Because the toxins are large protein molecules that insert into cellular membranes, similar results could be obtained if the toxins are "buffered" by the slice surface and did not reach the MF boutons (see DISCUSSION). We attempted to overcome the potential problem of tissue penetration by using

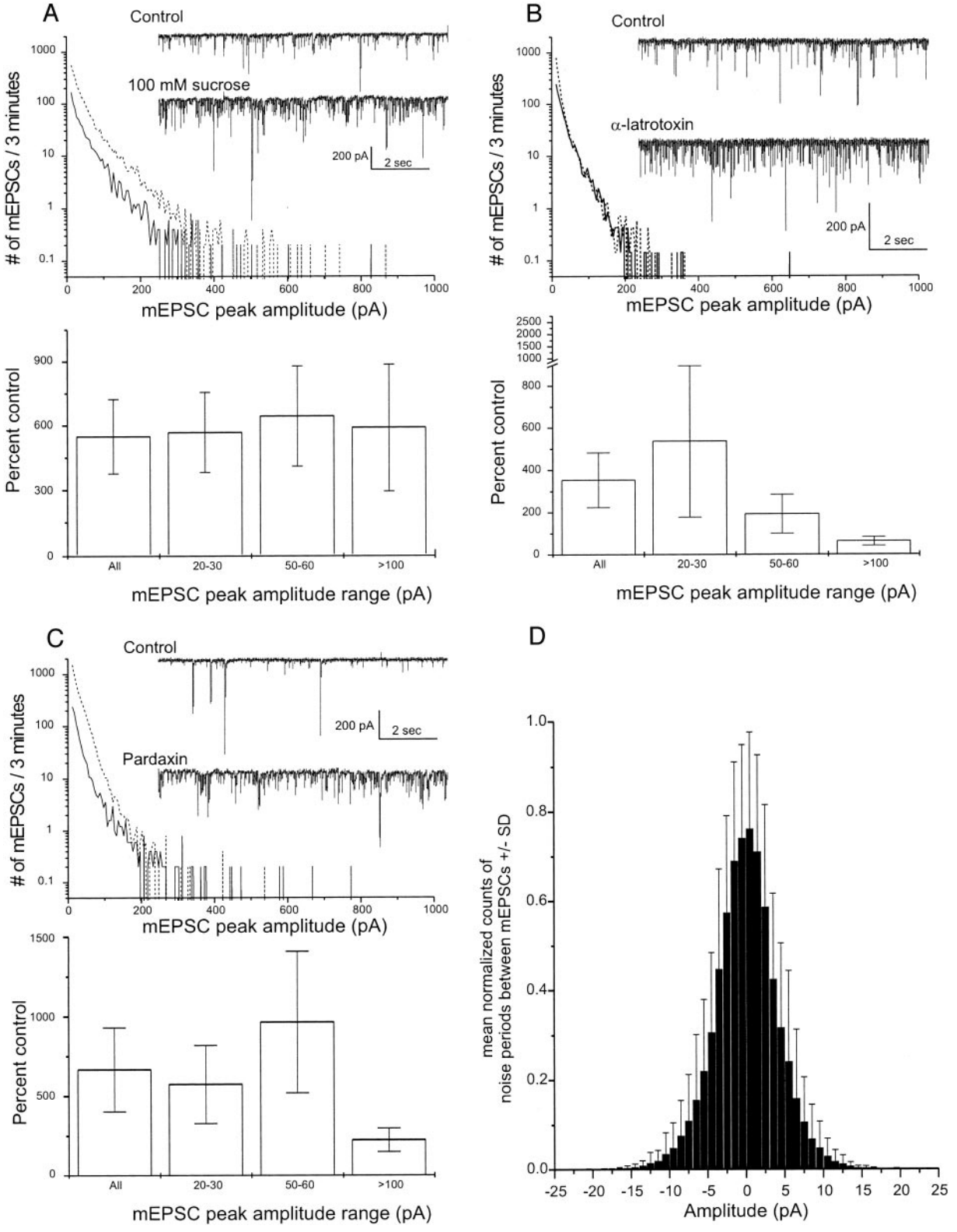

longer applications of the toxins; however, longer applications lead to such high rates of mEPSCs that individual mEPSCs could not be resolved.

Reduced temperature does not cause inflections on the rising phase of giant mEPSCs

If the giant mEPSCs are triggered by a signal that leads to a synchronous release of multiple vesicles, then lowering temperature should lead to a gradual desynchronization of the vesicular release. This predicted desynchronizing effect of lowering temperature has been reported for evoked transmission at the neuromuscular junction showing a variation in quantal delays from ~0.5 to >1 ms at 17.5°C with a Q_{10} of ~3 (Katz and Miledi 1965). A very broad range of quantal release delays (~0.6 to >4 ms) has also been observed in the calyx synapse of the medial nucleus of the trapezoid body in the CNS (Borst and Sakmann 1996). In the case of giant mEPSCs, "desynchronization" induced by low temperature would be reflected by either abolition of giant mEPSCs or an increase in the number of giant mEPSCs with inflected rising phases. This prediction was tested by recording mEPSCs from CA3 pyramidal cells while the temperature of the recording chamber was varied from 16 to 36°C. It should be noted that below a temperature of 15°C very few mEPSCs were observed and evoked synaptic transmission was abolished (unpublished observations) (Bénita and Condé 1972). Cooling to 16°C did not abolish giant mEPSCs, and the giant mEPSCs that were observed did not show any signs of increased rising-phase inflections. Figure 3 shows a plot of temperature versus the fraction of inflected giant mEPSCs. Each point in the plot represents the fraction of inflected giant mEPSCs at a given temperature (n = 31 recordings from 12 cells; see METHODS). A value equal to one means that all giant mEPSCs for that 3-min period were inflected. As can be seen, because there was no effect of temperature on the relative fraction of rising phase inflected giant mEPSCs ($R^2 = 0.31$; $P = 0.31$), these data indicate that the relative number of giant mEPSCs with inflected rising phases remains constant across a broad range of temperatures. This result supports the qualitative observation that although all mEPSCs were less frequent at cooler temperatures, giant mEPSCs were detected and often had smooth rising phases. In addition, this data set provides evidence that the spontaneous overlap of smaller mEPSCs does not account for occurrence of giant mEPSCs.

Based on these data, we conclude that there is no temperature-sensitive synchronization of multiple vesicular release that causes giant mEPSCs. However, the determination that giant mEPSCs often have inflected rising phases does suggest that those giant mEPSCs have nonstandard rising phase kinetics.

Giant mEPSCs are not calcium sensitive

If the giant mEPSCs are due to the synchronous release of multiple quanta, the synchronizing signal must be able to act rapidly over distances of a micron or more to access multiple release sites in the MF bouton (Chicurel and Harris 1992). A logical candidate for such a signal is a rapid elevation in intrabouton calcium that would then induce multivesicular release much like that which occurs when an action potential invades the MF bouton. In the case of the giant mEPSCs, the recording conditions eliminate the possibility that a sodium-dependent action potential provides the initial depolarization to initiate calcium influx via voltage-gated calcium channels (VGCCs). As a result, only two possible mechanisms remain that could lead to a spontaneous, fast elevation of presynaptic calcium: a spontaneous action potential solely mediated by VGCCs (Hagiwara et al. 1969) or a spontaneous release of calcium from some intracellular calcium store (Emptage et al. 2001; Llano et al. 2000).

Therefore we tested whether the occurrence of giant mEPSCs is affected by manipulations of both extracellular and intracellular calcium. Figure 4 summarizes the results of these experiments. We found that giant mEPSCs are insensitive to decreases in calcium influx either by removing extracellular calcium (Fig. 4*A*) or adding 100 μM cadmium (Fig. 4*B*). We also found that manipulation of intracellular calcium stores with caffeine (10 min @ 10 mM; Fig. 4*D*), cyclopiazonic acid (20–30 min @ 5–15 μM; Fig. 4*E*), or thapsigargin (20 min @ 1 μm; Fig. 4*F*) did not selectively reduce the frequency of giant mEPSCs (note that caffeine caused a generalized increase in the frequency of mEPSCs across all amplitudes). In addition ryanodine (30 min @10 μm; $n = 3$) had no specific effect on giant mEPSCs although all mEPSCs were slightly increased in frequency (126 ± 42%; data not shown). Finally, we attempted to buffer calcium in the presynaptic terminal using the membrane permeant calcium buffer BAPTA-AM. Similar to the other calcium manipulations, the application of BAPTA-AM (30–45 min @ 25 μM; Fig. 4*C*) did not reduce selectively the frequency of giant mEPSCs. Therefore we conclude that the generation of giant mEPSCs is independent of elevations in intracellular calcium due to influx through VGCCs or efflux from intracellular calcium stores.

FIG. 2. Effects of secretagogues on CA3 mEPSC amplitude distribution. *A*: effect of hypertonic (100 mOsm) sucrose. *Top*: average histogram of mEPSC peak amplitudes from 1-min recording epochs before (—) and during (- - -) local application of regular media made hyperosmotic with 100 mOsm of sucrose plotted on a logarithmic scale. *Inset, top*: 10 s from a control period of recording; *bottom*: recorded in the presence of sucrose. *A, bottom*: bar graph illustrating the mean percent change in mEPSC frequency as a function of mEPSC peak amplitude. Data are from 5 cells. All data in *A* were collected using a KGluc pipette solution. *B*: effect of 1 nM α-latrotoxin. *Top*: average histogram of mEPSC peak amplitudes from 3-min recording epochs before (—) and after (- - -) 20–30 min of 1 nM α-latrotoxin plotted on a logarithmic scale. *Inset, top*: 10 s from a control period of recording; *bottom*: recorded in the presence of α-latrotoxin. *B, bottom*: bar graph illustrating the mean percent change in mEPSC frequency as a function of mEPSC peak amplitude. Data are from 6 cells. *C*: effect of 1–2 nM Pardaxin. *Top*: average histogram of mEPSC peak amplitudes from 3-min recording epochs before (—) and after (- - -) 15–30 min of 1–2 nM pardaxin plotted on a logarithmic scale. *Inset, top*: 10 s from a control period of recording; *bottom*: recorded in the presence of pardaxin. *C, bottom*: Bar graph illustrating the mean percent change in mEPSC frequency as a function of mEPSC peak amplitude. Data are from 5 cells. *D*: histogram of average baseline noise between mEPSCs (±SD). The difference between the mean of the trace and each digitized sample was calculated for the longest interval from each data file used in Figs. 2, 4, and 5 was binned into 1-pA bins and normalized to the most populated bin. The average of these resulting normalized histograms is shown here.

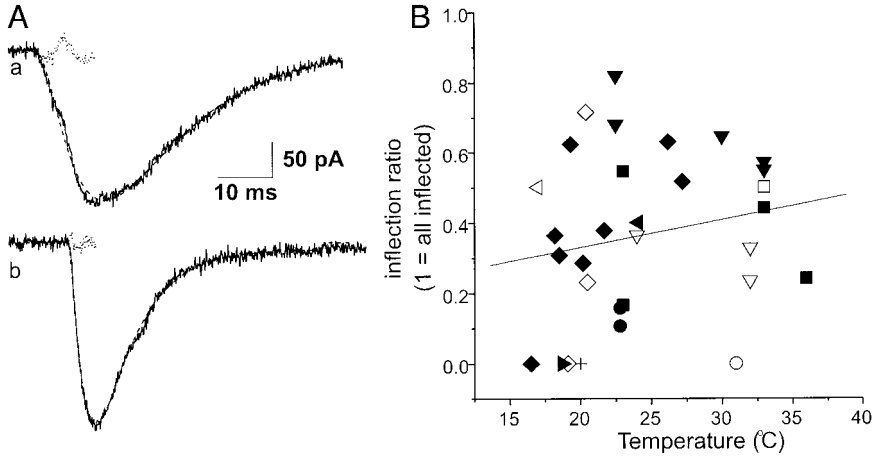

FIG. 3. Decreasing temperature does not reveal an increase in rising phase inflections for giant mEPSCs. *A*: quantification of rising phase inflections in mEPSC. mEPSCs were fit with a sum of 2 squared exponentials function, and the fit residuals were used to quantify rising phase inflections. *a*: a selected mEPSC recorded at 22.5°C (—) with an obvious inflection during its rising phase was fit using the equation described in METHODS (- - -). The difference (or residuals) between the rising phase of the raw data and the best fit fit is also shown (· · ·). Note that the residuals trace is not a simple straight line that is indicative of an inflection on the rising phase of the mEPSC. *b*: another selected mEPSC from a different recording at 19°C had no obvious inflections during its rising phase. The lines are the same as in *a*. Notice that the residuals in *b* are a straight line reflecting the lack of the rising phase inflections. *B*: each point in the plot represents the number of mEPSCs that exceeded the threshold value for being considered inflected for that recording (12 cells for a total of 31 recordings) at the given temperature (see METHODS). Symbol shapes indicate recordings from a single cell at different temperatures. The line is the best linear fit through the data. The R^2 value for the fit is 0.0361 with a P value of 0.31.

Blockade of AMPA-Rs lacking the GluR-B subunit does not inhibit giant mEPSCs

An alternative postsynaptic mechanism for giant mEPSCs is the presence of large-conductance AMPA-Rs at the MF synapse. It is known that AMPA-Rs, which lack the GluR-B subunit, may have as much as a threefold higher single-channel conductance (20–30 pS) than the AMPA-Rs containing the GluR-B subunit. However, when membrane patches are pulled from the proximal apical dendrite in the region of the MF synapses, the receptors encountered are typical of AMPA-Rs from elsewhere in the dendritic tree with a single channel conductance of 8.5–10 pS (Jonas et al. 1993; Spruston et al. 1995). The best evidence that AMPA-Rs at the MF synapse contain the GluR-B subunit is found in immunohistochemical studies which have shown GluR-B positive staining at this synapse (Blumcke et al. 1995; Petralia and Wenthold 1992; Siegel et al. 1995).

It is possible that a subset of the MF synaptic sites might lack the GluR-B subunit and therefore lead to the generation of the giant mEPSCs. This possibility was tested by examining the effect of 1 mM spermine on the frequency of giant mEPSCs because it has been shown that at this concentration, extracellular spermine can block AMPA-Rs, which lack the GluR-B subunit (Washburn and Dingledine 1996). Figure 5 demonstrates that spermine does not cause the decrease in the frequency of giant mEPSCs that would be expected if they are mediated via GluR-B lacking receptors. Instead, 15- to 35-min applications of 1 mM spermine had the unexpected outcome of increasing the frequency of all mEPSCs regardless of their peak amplitude. The increase in mEPSC frequencies had a gradual onset that stabilized between 15 and 20 min. Spermine (1 mM) increased the frequency of all mEPSCs detected by 419 ± 81% (Student's 1-tailed *t*-test, $P = 0.006$; $n = 5$). Considered separately, the giant mEPSCs were increased by 431 ± 149% (Student's 1-tailed *t*-test, $P = 0.034$; $n = 5$). It is concluded that the MF giant mEPSCs are not mediated by activation of AMPA-Rs lacking the GluR-B subunit.

Anatomical evidence for a monovesicular mechanism for giant mEPSCs

An alternative presynaptic mechanism for giant mEPSC generation is to increase the size of glutamatergic vesicles. There is some evidence for this mechanism potentially occurring at the MF synapses. Although the mean diameter of the small clear vesicles in the MF boutons has been reported to be the same as in non-MF boutons (35–45 nm) (Amaral and Dent 1981; Harris and Sultan 1995), MF boutons also have some unusually large clear vesicle-like structures (Amaral and Dent 1981). Although the large clear vesicles in the MF bouton have not been quantitatively analyzed, they have been reported to be ≤200 nm in diameter. It is not known whether these vesicles contain glutamate.

If we assume that the contents from a vesicle with the mean diameter of 40 nm (Amaral and Dent 1981) generate a mean mEPSC with an observed peak conductance of 133 pS (Jonas et al. 1993), then vesicles with diameters on the order of 100 nm are required to generate a giant mEPSC with a peak conductance of 2 nS. Therefore we examined MF boutons at the electronmicroscopic level to determine the frequency and spatial distribution of putatively glutamatergic vesicles to determine if unusually large vesicles exist in sufficient numbers to explain giant mEPSCs. Figure 6 compares electromicrographs from active zones in a MF bouton (Fig. 6, *A* and *C*) and in a non-MF bouton (Fig. 6, *B* and *D*) Several large clear vesicles are docked presynaptically at the MF bouton (Fig. 6*C*, arrows). We divided the clear vesicles into three different categories: docked, proximal nondocked, and distal. Figure 7 shows the distributions of vesicle diameters observed from multiple active zones from four different boutons in a single EM series. The docked and proximal nondocked pools have a

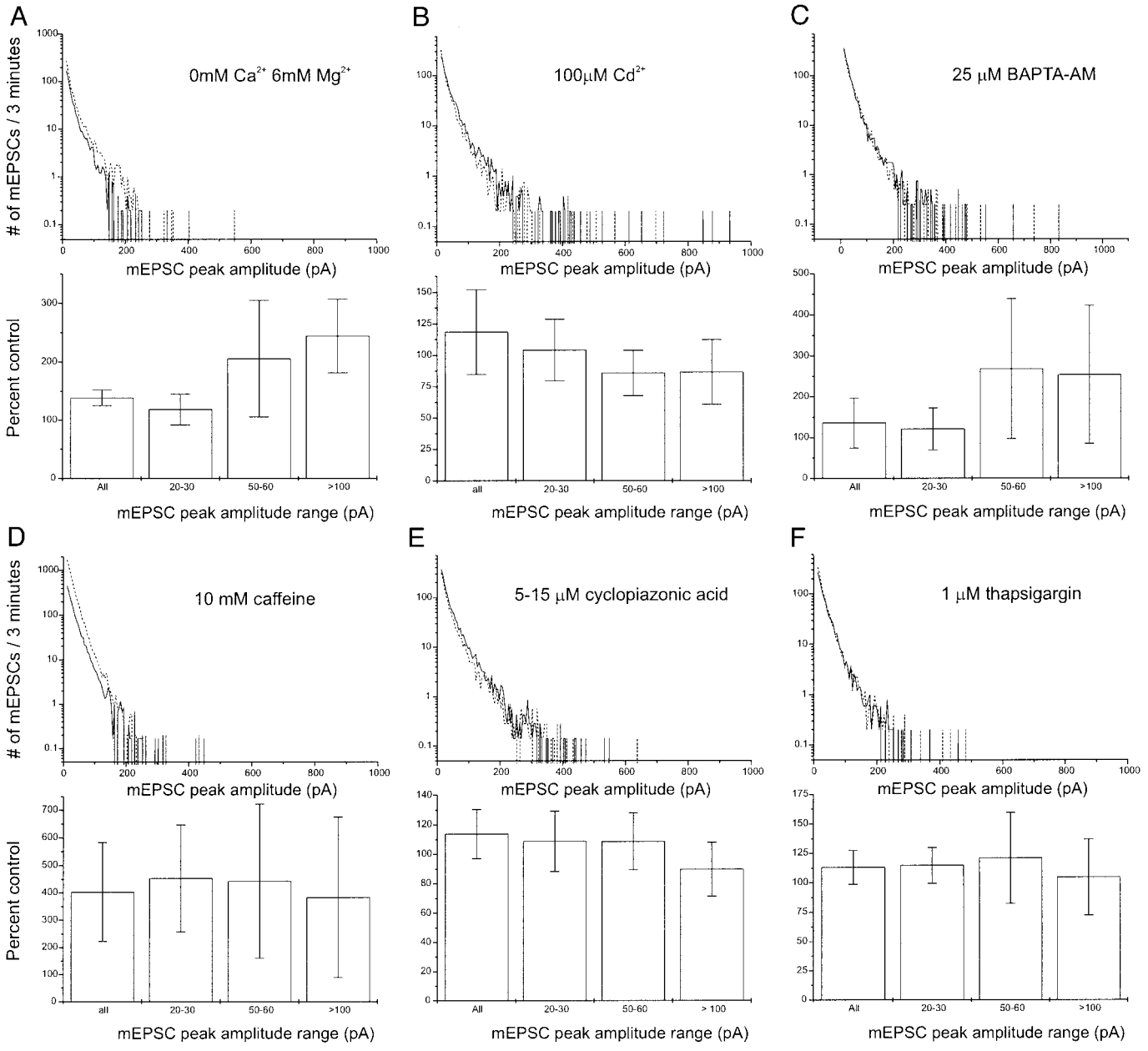

FIG. 4. Giant mEPSCs are not calcium sensitive. *A*: effect of superfusion of artificial cerebrospinal fluid (ACSF) containing 0 mM calcium and 6 mM magnesium. *Top*: average histogram of mEPSC peak amplitudes before (—) and 5–15 min after (- - -) changing divalent concentration from 3 mM calcium and 3 mM magnesium to 0 mM calcium and 6 mM magnesium plotted on a logarithmic scale. *Bottom*: bar graph illustrating the percent change in mEPSC frequency as a function of mEPSC peak amplitude. Results are averages from 5 cells. *B*: effect of 100 μM cadmium. Data are from 5 cells, 3 obtained with CsGluc electrode solution and 2 obtained with KGluc electrode solution. *C*: effect of 25 μM BAPTA-AM in 0.1% DMSO, 1.3 mM 2-hydroxypropyl-γ-cyclodextrin, and 1 mM probenecid. Data are from 4 cells. *D*: effect of 10 mM Caffeine. Data are from 6 cells. *E*: effect of 5–15 μM cyclopiazonic acid in 0.01% DMSO. Data are from 7 cells. *F*: effect of 1 μM thapsigargin in 0.1% DMSO. Data are from 5 cells.

strong skew of vesicle diameters up to 150 nm while the distal vesicle pool has a distribution of small vesicle diameters similar to what is observed at the Schaffer collateral synapses in area CA1 (Harris and Sultan 1995).

If giant mEPSCs are due to the release of giant vesicles, then there must be a sufficient number of postsynaptic glutamate receptors to respond to the glutamate without saturating. A MF synaptic complex with 12 PSDs has been demonstrated to have 40 times the PSD area (and therefore 40 times the number of available glutamate receptors) of a single CA1 synapse (Chicurel and Harris 1992; Harris and Stevens 1989). It also has been shown that glutamate can diffuse out of the MF synaptic complex to interact with other MF synaptic complexes (Min et al. 1998; Schmitz et al. 2000; Vogt and Nicoll 1999). This suggests that following the release of a large amount of glutamate from any given release site in the MF synaptic complex, multiple PSDs and their associated glutamate receptors will be activated before glutamate can diffuse out of the complex or be taken up via active pumps. A prediction of this hypothesis is that the rise times and decay time constants of giant MF

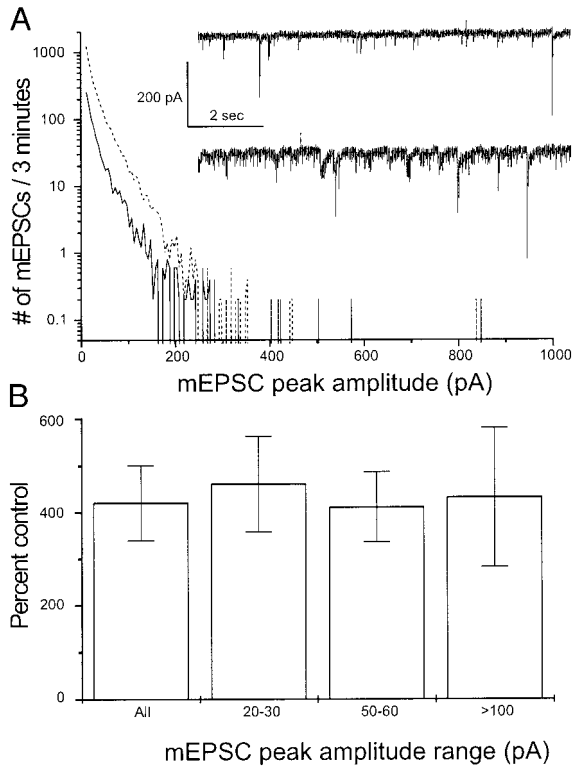

FIG. 5. Blockade of AMPA-Rs lacking the GluR-B subunit with spermine does not inhibit giant mEPSCs. *A*: average histogram of mEPSC peak amplitudes from 3-min recording epochs before (—) and after (- - -) 15–35 min of 1 mM spermine plotted on a logarithmic scale. *Inset, top*: 10 s from a control period of recording; *bottom*: recorded in the presence of spermine. *B*: bar graph illustrating the mean percent change in mEPSC frequency as a function of mEPSC peak amplitude. The percent changes for each recording are given by the points on the bar graph. Data are from 5 cells.

mEPSCs should generally be longer than for smaller mEPSCs. Examination of mEPSC peak amplitude versus 20–80% rise time or decay tau (Fig. 8, *A* and *C*) demonstrates that there is no clear overall relationship between mEPSC amplitude and 20–80% rise time or decay tau. However, as mEPSC peak amplitude increases, the minimum observed 20–80% rise time and decay tau for a given mEPSC amplitude range becomes progressively longer (Fig. 8, *B* and *D*; 5 of 5 cells examined). This is opposite to the expected relationship if only electrotonic filtering is responsible for variation in rise and decay time. Whereas this observation does not provide direct evidence regarding glutamate spillover inside the MF synaptic complex, it is consistent with that hypothesis and is indicative of a large amount of glutamate being released that takes longer to diffuse away from the release site.

DISCUSSION

We have found that the giant mEPSCs that arise from the MF synapses onto CA3 pyramidal cells are not due to synchronous multivesicular release within MF boutons nor activation of higher conductance postsynaptic AMPA channels lacking the GluR-B subunit. Our data also suggest that all vesicles are spontaneously released via a calcium-independent release mechanism. As an alternative to synchronous multivesicular release, we have found that giant clear vesicles exist in the MF boutons in sufficient numbers to account for the occurrence of giant mEPSCs. Therefore we hypothesize that giant mEPSCs arise from the release of glutamate from single large clear vesicles.

Evidence against a multivesicular mechanism for giant mEPSCs

The anatomical presence of multiple release sites between a single MF bouton and a CA3 pyramidal cell and the data obtained with α-LTX and PDX would suggest that multivesicular release synchronized by calcium is responsible for the occurrence of giant mEPSCs. However, our series of experiments designed to test that an increase in intrabouton calcium synchronizes multivesicular release generally failed to support this mechanism. Since calcium is the only known fast-acting trigger and is believed to be the last step prior to vesicle release, we need to reconsider the interpretation of the data obtained with α-LTX and PDX by taking into account two possible confounding variables that originate from the recording method and preparation. The first confounding variable is that these two toxins are very large molecules, α-LTX is 130 kDa, and PDX is 3 kDa. As a result of the large molecular size and the complex morphology of the MF bouton, it is possible that the toxins were

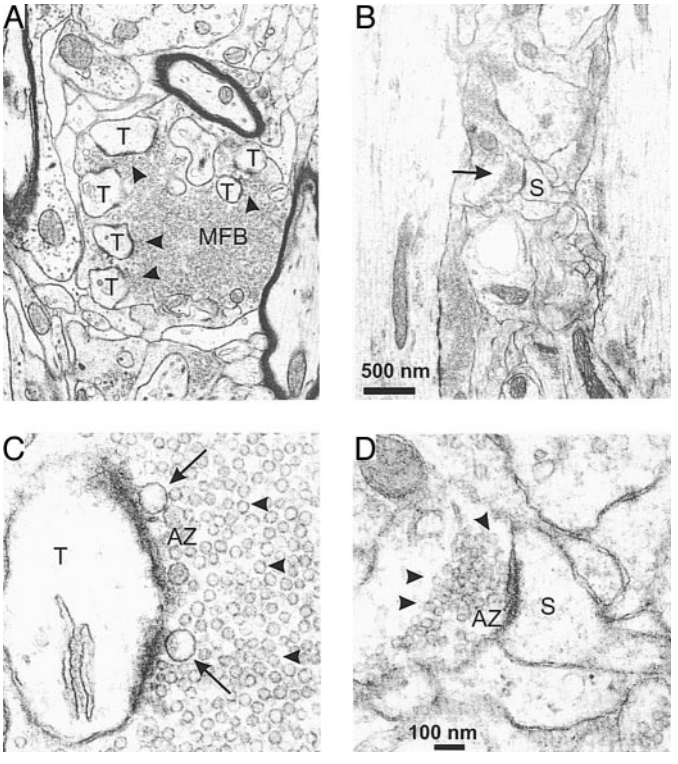

FIG. 6. Large clear vesicles are present in MF boutons. *A*: electronmicrograph showing a section through a mossy fiber bouton. The mossy fiber bouton (MFB) is filled with numerous small clear vesicles and a few larger clear vesicles that tend to cluster around active zones (▲) associated with processes from the thorny excrescence of a CA3 pyramidal cell (T). *B*: a electronmicrograph showing a section through a nonmossy fiber bouton from the same EM series. *C*: higher-resolution section of a mossy fiber active zone. ▲, example small clear vesicles and arrows indicate examples of large clear vesicles. *D*: higher-resolution section of a nonmossy fiber synaptic active zone with a spine (S). ▲, example small clear vesicles. Notice that the small clear vesicles are much more homogeneous in their diameter than in *C*. Scale bar is 500 nm in *A* and *B* and 100 nm in *C* and *D*.

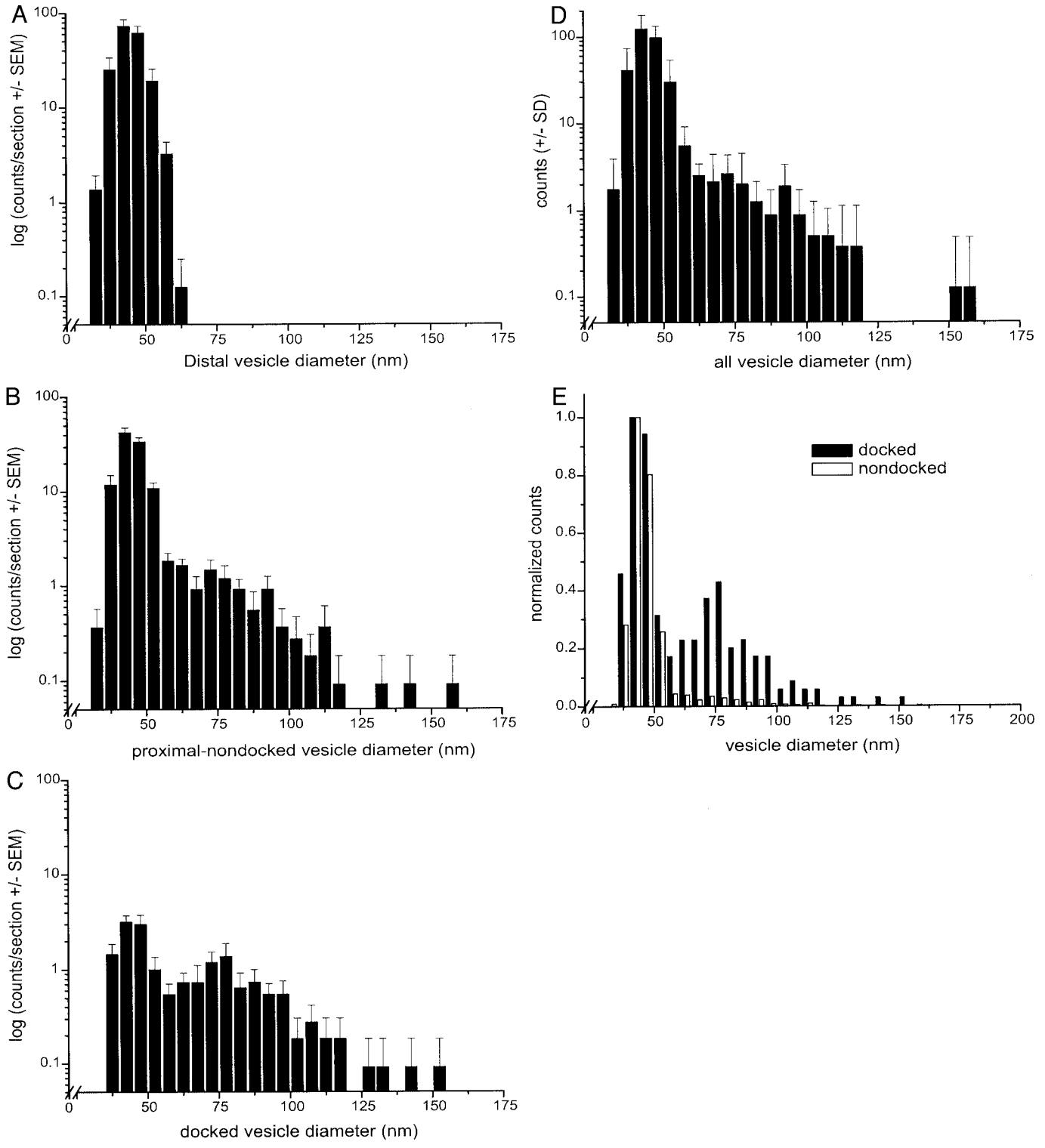

FIG. 7. Large clear vesicles are present in significant numbers and are found close to the active zone. *A*: average distribution of distal (to the active zone) vesicle diameters. *B*: average distribution of proximal-nondocked vesicle diameters. *C*: average distribution of docked vesicle diameters. *A–C* are means ± SE and plotted on a logarithmic scale. *D*: average distribution of all vesicle diameters over entire bouton (±SD). *A* and *D* are from 8 active zones from 4 separate boutons. *B* and *C* are from 11 different active zones from the 4 separate boutons. *E*: normalized average histograms of docked (■) vs. nondocked (▨) vesicles. Note that the docked pool has a relatively higher ratio of large- to small-diameter vesicles compared with the nondocked.

unable to reach the synaptic release sites where they are believed to be exert their actions. Specifically, the blind whole cell methods used in these studies resulted in recordings from the somas of CA3 pyramidal cells deep in the slice (100–200 μm below the slice surface). Due to its proximity to the soma, the MF synaptic region on the proximal apical

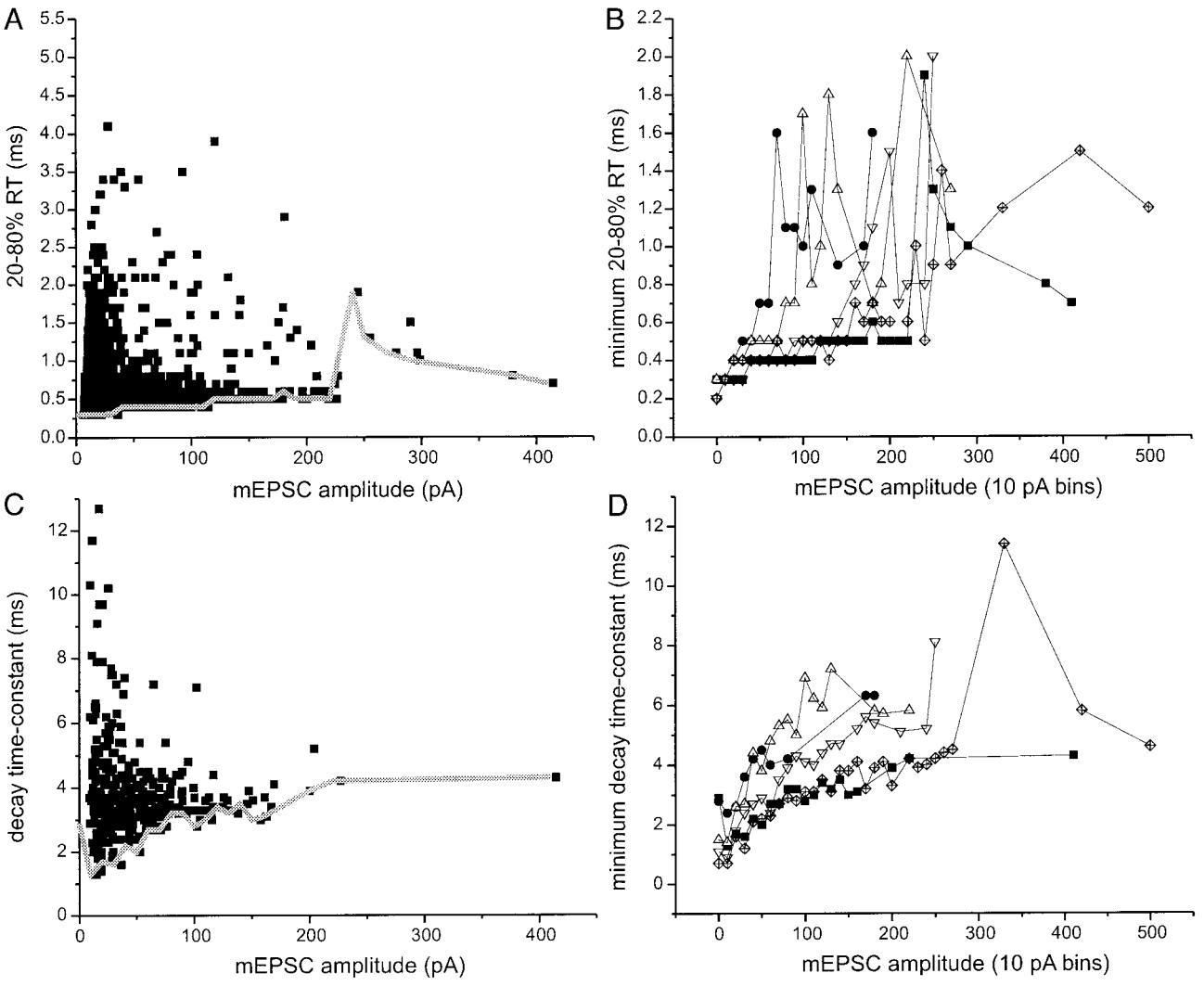

FIG. 8. Giant mEPSCs do not have fast rising and decay kinetics. *A*: mEPSC 20–80% rise time (RT) vs. amplitude for all mEPSCs from a single representative recording from a CA3 pyramidal cell. The gray line indicates the fastest 20–80% rise time recorded over 10-pA amplitude bins. *B*: the fastest 20–80% rise time recorded over 10-pA amplitude bins for all 5 cells examined. The gray line in *A* is replotted as black squares. *C*: mEPSC decay time constants vs. amplitude from the same representative CA3 pyramidal cell. The decay phase of each mEPSC that did not have another overlapping mEPSC was fit with a single exponential. The gray line indicates the fastest decay time constant recorded over 10-pA amplitude bins. *D*: the fastest decay time constant recorded over 10-pA amplitude bins for all 5 cells examined. The gray line in *C* is replotted as the black squares.

dendrites also would be deep in the slice, which would prevent the toxins from reaching the MF boutons. The fact that the smaller toxin, PDX, was able to increase slightly the frequency of giant mEPSCs suggests that a size dependent penetration of the toxins may have occurred. The second confounding variable is that both of the toxins have been reported to be able to partition into the membrane and form pores. As a result, it is likely that the surface tissue of the slice acted as a buffer further reducing the concentration of toxin that was reached in the middle of the slice where the MF terminals on the recorded cell were located. In contrast, the non-MF synapses are located on the dendritic branches that are located throughout the depth of the slice with the most superficial branches and synapses being exposed to the highest concentration of toxin.

The experiment using hypertonic sucrose is not subject to the same problems of tissue penetration and conclusively demonstrate that mEPSCs of all amplitudes are increased in frequency. It is believed that hypertonic sucrose induces vesicular release by lowering the energy barrier for spontaneous release (Rosenmund and Stevens 1996). The proposed lower energy barrier mechanism suggests that it is not likely that the hypertonic sucrose would induce synchronized multivesicular release across multiple release sites/active zones. Therefore results from these experiments provide strong evidence against a multivesicular-multiple release mechanism leading to giant mEPSCs. Similarly, the unexpected facilitatory effects of spermine and caffeine on mEPSC frequency were uniform across mEPSC amplitude. Together these data suggest that all mEPSCs at all peak amplitudes share at least one common point of modulation.

Our results differ those from a recent study at the inhibitory synapse between cerebellar interneurons and Purkinje cells (Llano et al. 2000). That study concludes that the largest mIPSCs recorded in the Purkinje cells result from the synchronous release of multiple vesicles triggered by spontaneous

release of calcium from intracellular stores. In contrast, our experiments at the MF synapse manipulating intraterminal calcium suggest that the giant mEPSCs at the hippocampal mossy fiber excitatory synapse are not produced by a calcium-dependent synchronization mechanism. Whether this lack of similarity in the release mechanism of very large spontaneous events is due to general differences between excitatory and inhibitory synapses or to specific differences between the two types of synapses remains to be investigated.

Evidence for single large vesicles underlying giant mEPSCs

If the giant mEPSCs are due to giant vesicles releasing large amounts of glutamate, then there must also be a sufficient number of postsynaptic receptors to detect the increased levels of glutamate without receptor saturation. If we assume that AMPA-Rs from the MF synaptic region have a single-channel conductance of 8.5–10 pS for (Jahr and Stevens 1987; Jonas et al. 1993; Spruston et al. 1995), then 2,100–2,500 AMPA-Rs must have opened for the largest giant mEPSC (21 nS) and 400–470 AMPA-Rs must have opened for the mean largest giant mEPSC (4 nS). This is compared with the 20–150 channels mediating the accepted quantal mEPSC size at a variety of other cortical synapses (Bekkers and Stevens 1989; Hestrin 1992; Jack et al. 1994; Kullman 1993). The number of AMPA-Rs exposed to glutamate during a giant mEPSC is certain to be higher because the maximal AMPA-R probability of opening is 0.71 (Hestrin 1992; Jonas et al. 1993).

Recent experiments have suggested that AMPA-Rs at non-MF synapses in culture are not saturated by the release of normal small clear vesicles containing glutamate (Liu et al. 1999; McAllister and Stevens 2000). There are three reasons why the released glutamate at the MF synapses is even less likely to produce saturation. The first reason why AMPA-Rs do not saturate is that there may be a higher density of AMPA-Rs in the PSDs associated with the MFs. This is possible because the MF synapse is believed to lack or at least have a reduced number of NMDA receptors (Harris and Cotman 1986; Monaghan and Cotman 1985; but see Weisskopf and Nicoll 1995). It is possible that the extra space in a MF PSD resulting from a reduced number of NMDA receptors is filled up by AMPA-Rs. However, this possibility also cannot account for a 100-fold range in mEPSC amplitudes. The second reason is that the average area of the PSD at the MF synapse is three times as large as that in CA1 (0.22 vs. 0.069 μm^2, respectively) (Chicurel and Harris 1992; Harris and Stevens 1989). If PSD area is correlated with the number of glutamate receptors, then there should be, on average, three times as many glutamate receptors at MF PSDs. However, as previously noted, the maximal PSD size is the same for both CA1 and the MFs; this suggests that differences in PSD area cannot solely account for the occurrence of giant mEPSCs ($\leq$0.54 μm^2) (Chicurel and Harris 1992; Harris and Stevens 1989). Finally, as mentioned previously, the MF synaptic complex has multiple PSDs, each with its own complement of glutamate receptors. Our data concerning the relatively slower decay time constants of the giant mEPSCs would support the idea that glutamate spillover occurs between the individual synaptic clefts within the MF synaptic complex. The spillover hypothesis may also account for the apparent temperature-independent inflections of giant mEPSC rising phases. The diffusion of glutamate inside the MF synaptic complex may lead to the appearance of rising phase inflections that might otherwise be considered a sign of asynchronous multivesicular release. Specifically, rising phase inflections could occur as the leading edge of the wave of glutamate inside the MF synaptic complex travels from regions of low to high AMPA-R density.

We believe that the most parsimonious interpretation of our data is that giant mEPSCs are due to the release of single large clear vesicles from the MF bouton. However, we recognize that several critical aspects of this hypothesis remain to be investigated. For example, do the large vesicles observed in the EM micrographs contain glutamate? Do the large vesicles express the necessary release apparatus proteins in their membrane? The ultimate test will be to find a way to manipulate selectively the number of large clear vesicles and then observe the expected changes in the occurrence of giant mEPSCs.

Functional implications of giant mEPSCs

Giant mEPSCs may play an important role in modulating background levels of neuronal activity in the intact brain. A recent study has demonstrated that minis can be recorded from cortical cells in vivo when all synaptic transmission is blocked by infusion of TTX (Pare et al. 1997), indicating that minis are not an artifact of in vitro preparations. It has been demonstrated that the levels of synaptic activity can influence the input/output functions of neurons in a network as predicted by stochastic resonance theory (Burnod and Korn 1989). A physiological role for mEPSPs in CNS function is further supported by findings that several neuromodulators such as dopamine (Momiyama et al. 1996), enkephalin (Cohen et al. 1992), adenosine, and GABA (Scanziani et al. 1992) can modulate mEPSP frequency in a variety of in vitro preparations. These changes in excitatory "tone" would be independent of the firing activity of the synaptic inputs. The stochastic resonance theory mentioned above generally assumes that the mini activity does not directly lead to depolarization of neurons past action potential threshold. However, the membrane potential of CA3 pyramidal cells in vivo has been reported to rest at about -60 mV (Li et al. 1994). Given that giant mEPSPs can be $\leq$10 mV in amplitude, it would expected that individual giant mEPSPs would depolarize the postsynaptic cell enough to reach threshold for an action potential. This allows for the intriguing possibility of MF driven activation of CA3 pyramidal cells in the absence of granule cell spiking.

We thank N. Urban for providing the current-clamp traces in Fig. 1 and M. Feinberg for preparing new serial EM sections.

This work was supported by National Institutes of Health Grants MH-10474 (to D. A. Henze), NS-24288 (to G. Barrionuevo), and NS-21184 and MH/DA-57351 (to K. M. Harris).

REFERENCES

AGHAJANIAN GK AND RASMUSSEN K. Intracellular studies in the facial nucleus illustrating a simple new method for obtaining viable motoneurons in adult rat brain slices. *Synapse* 3: 331–338, 1989.

AMARAL DG AND DENT JA. Development of the mossy fibers of the dentate gyrus. I. A light and electron microscopic study of the mossy fibers and their expansions. *J Comp Neurol* 195: 51–86, 1981.

ANKRI N, LEGENDRE P, FABER DS, AND KORN H. Automatic detection of spontaneous synaptic responses in central neurons. *J Neurosci Methods* 52: 87–100, 1994.

BEKKERS JM, RICHERSON GB, AND STEVENS CF. Origin of variability in quantal size in cultured hippocampal neurons and hippocampal slices. *Proc Natl Acad Sci USA* 87: 5359–5362, 1990.

BEKKERS JM AND STEVENS CF. NMDA and non-NMDA receptors are co-localized at individual excitatory synapses in cultured rat hippocampus. *Nature* 341: 230–233, 1989.

BEKKERS JM AND STEVENS CF. Cable properties of cultured hippocampal neurons determined from sucrose-evoked miniature EPSCs. *J Neurophysiol* 75: 1250–1255, 1996.

BENITA M AND CONDE H. Effects of local cooling upon conduction and synaptic transmission. *Brain Res* 36: 133–151, 1972.

BLANTON MG, LOTURCO JJ, AND KRIEGSTEIN AR. Whole cell recording from neurons in slices of reptilian and mammalian cerebral cortex. *J Neurosci Methods* 30: 203–210, 1989.

BLUMCKE I, WOLF HK, HOF PR, MORRISON JH, AND WIESTLER OD. Regional distribution of the AMPA glutamate receptor subunits GluR2(4) in human hippocampus. *Brain Res* 682: 239–244, 1995.

BOLSHAKOV VY AND SIEGELBAUM SA. Regulation of hippocampus transmitter release during development and long-term potentiation. *Science* 269: 1730–1734, 1995.

BORST JG AND SAKMANN B. Calcium influx and transmitter release in a fast CNS synapse. *Nature* 383: 431–434, 1996.

BROWN TH, WONG RKS, AND PRINCE DA. Spontaneous miniature synaptic potentials in hippocampal neurons. *Brain Res* 177: 194–199, 1979.

BROWN TH AND JOHNSTON D. Voltage-clamp analysis of mossy fiber synaptic input to hippocampal neurons. *J Neurophysiol* 50: 487–507, 1983.

BURNOD Y AND KORN H. Consequences of stochastic release of neurotransmitters for network computation in the central nervous system. *Proc Natl Acad Sci USA* 86: 352–356, 1989.

CAPOGNA M, GAHWILER BH, AND THOMPSON SM. Calcium-independent actions of alpha-latrotoxin on spontaneous and evoked synaptic transmission in the hippocampus. *J Neurophysiol* 76: 3149–3158, 1996.

CHICUREL ME AND HARRIS KM. Three-dimensional analysis of the structure and composition of CA3 branched dendritic spines and their synaptic relationships with mossy fiber boutons in the rat hippocampus. *J Comp Neurol* 325: 169–182, 1992.

COHEN GA, DOZE VA, AND MADISON DV. Opioid inhibition of GABA release from presynaptic terminals of rat hippocampal interneurons. *Neuron* 9: 325–335, 1992.

EMPTAGE NJ, REID CA, AND FINE A. Calcium stores in hippocampal synaptic boutons mediate short-term plasticity, store-operated Ca^{2+} entry, and spontaneous transmitter release. *Neuron* 29: 197–208, 2001.

GRAY R, RAJAN AS, RADCLIFFE KA, YAKEHIRO M, AND DANI JA. Hippocampal synaptic transmission enhanced by low concentrations of nicotine. *Nature* 383: 713–716, 1996.

HAGIWARA S, HAYASHI H, AND TAKAHASHI K. Calcium and potassium currents of the membrane of a barnacle muscle fibre in relation to the calcium spike. *J Physiol (Lond)* 205: 115–129, 1969.

HAMLYN LH. The fine structure of the mossy fibre endings in the hippocampus of the rabbit. *J Anat* 96: 112–126, 1962.

HARRIS EW AND COTMAN CW. Long-term potentiation of guinea pig mossy fiber responses is not blocked by N-methyl D-aspartate antagonists. *Neurosci Lett* 70: 132–137, 1986.

HARRIS KM AND STEVENS JK. Dendritic spines of CA1 pyramidal cells in the rat hippocampus: serial electron microscopy with reference to their biophysical characteristics. *J Neurosci* 9: 2982–2997, 1989.

HARRIS KM AND SULTAN P. Variation in the number, location and size of synaptic vesicles provides an anatomical basis for the nonuniform probability of release at hippocampal Ca1 synapses. *Neuropharmacology* 34: 1387–1395, 1995.

HENZE DA, CAMERON WE, AND BARRIONUEVO G. Dendritic morphology and its effects on the amplitude and rise-time of synaptic signals in hippocampal CA3 pyramidal cells. *J Comp Neurol* 369: 331–344, 1996.

HENZE DA, CARD JP, BARRIONUEVO G, AND BEN-ARI Y. Large amplitude miniature excitatory postsynaptic currents in hippocampal CA3 pyramidal neurons are of mossy fiber origin. *J Neurophysiol* 77: 1075–1086, 1997.

HENZE DA, URBAN NN, AND BARRIONUEVO G. The multifarious hippocampal mossy fiber pathway: a review. *Neuroscience* 98: 407–427, 2000.

HESTRIN S. Activation and desensitization of glutamate-activated channels mediating fast excitatory synaptic currents in the visual cortex. *Neuron* 9: 991–999, 1992.

HESTRIN S, SAH P, AND NICOLL RA. Mechanisms generating the time course of dual component excitatory synaptic currents recorded in hippocampal slices. *Neuron* 5: 247–253, 1990.

JACK JJB, LARKMAN AU, MAJOR G, AND STRATFORD KJ. Quantal analysis of the synaptic excitation of CA1 hippocampal pyramidal cells. In: *Molecular and Cellular Mechanisms of Neurotransmitter Release*, edited by Stjarne L, Greengard P, Grillner S, Hokfelt T, and Ottoson D. New York: Raven, 1994, p. 275–299.

JAHR CE AND STEVENS CF. Glutamate activates multiple single channel conductances in hippocampal neurons. *Nature* 325: 522–525, 1987.

JONAS P, MAJOR G, AND SAKMANN B. Quantal components of unitary EPSCs at the mossy fibre synapse on CA3 pyramidal cells of rat hippocampus. *J Physiol (Lond)* 472: 615–663, 1993.

KATZ B AND MILEDI R. The effect of temperature on the synaptic delay at the neuromuscular junction. *J Physiol (Lond)* 181: 656–670, 1965.

KORN H, BAUSELA F, CHARPIER S, AND FABER DS. Synaptic noise and multiquantal release at dendritic synapses. *J Neurophysiol* 70: 1249–1254, 1993.

KORN H, SUR C, CHARPIER S, LEGENDRE P, AND FABER DS. The one-vesicle hypothesis and multivesicular release. *Adv Second Messenger Phosphoprotein Res* 29: 301–322, 1994.

KULLMANN DM. Quantal variability of excitatory transmission in the hippocampus: implications for the opening probability of fast glutamate-gated channels. *Proc R Soc Lond B Biol* 253: 107–116, 1993.

LANGDON RB, JOHNSON JW, AND BARRIONUEVO G. Posttetanic potentiation and presynaptically induced long-term potentiation at the mossy fiber synapse in rat hippocampus. *J Neurobiol* 26: 370–385, 1995.

LAZAROVICI P AND LELKES PI. Pardaxin induces exocytosis in bovine adrenal medullary chromaffin cells independent of calcium. *J Pharmacol Exp Therap* 263: 1317–1326, 1992.

LI X-G, SOMOGYI P, YLINEN A, AND BUZSÁKI G. The hippocampal CA3 network: an in vivo intracellular labeling study. *J Comp Neurol* 339: 181–208, 1994.

LIU G, CHOI S, AND TSIEN RW. Variability of neurotransmitter concentration and nonsaturation of postsynaptic AMPA receptors at synapses in hippocampal cultures and slices. *Neuron* 22: 395–409, 1999.

LLANO I, GONZALEZ J, CAPUTO C, LAI FA, BLAYNEY LM, TAN YP, AND MARTY A. Presynaptic calcium stores underlie large-amplitude miniature IPSCs and spontaneous calcium transients. *Nat Neurosci* 3: 1256–1265, 2000.

MAJOR G, LARKMAN AU, JONAS P, SAKMANN B, AND JACK JJB. Detailed passive cable models of whole-cell recorded CA3 pyramidal neurons in rat hippocampal slices. *J Neurosci* 14: 4613–4638, 1994.

MALGAROLI A AND TSIEN RW. Glutamate-induced long-term potentiation of the frequency of miniature synaptic currents in cultured hippocampal neurons. *Nature* 357: 134–139, 1992.

MANABE T, RENNER P, AND NICOLL RA. Postsynaptic contribution to long-term potentiation revealed by the analysis of miniature synaptic currents. *Nature* 355: 50–55, 1992.

MCALLISTER AK AND STEVENS CF. Nonsaturation of AMPA and NMDA receptors at hippocampal synapses. *Proc Natl Acad Sci USA* 97: 6173–6178, 2000.

MIN MY, RUSAKOV DA, AND KULLMANN DM. Activation of AMPA, kainate, and metabotropic receptors at hippocampal mossy fiber synapses: role of glutamate diffusion. *Neuron* 21: 561–570, 1998.

MOMIYAMA T, SIM JA, AND BROWN DA. Dopamine D-1-like receptor-mediated presynaptic inhibition of excitatory transmission onto rat magnocellular basal forebrain neurones. *J Physiol (Lond)* 495: 97–106, 1996.

MONAGHAN DT AND COTMAN CW. Distribution of N-methyl-D-aspartate-sensitive L-[3H]glutamate-binding sites in rat brain. *J Neurosci* 5: 2909–2919, 1985.

O'REILLY RC AND MCCLELLAND JL. Hippocampal conjunctive encoding, storage, and recall: avoiding a trade-off. *Hippocampus* 4: 661–682, 1994.

PARE D, LEBEL E, AND LANG EJ. Differential impact of miniature synaptic potentials on the soma and dendrites of pyramidal neurons in vivo. *J Neurophysiol* 78: 1735–1739, 1997.

PERIYASAMY S, KOTHAPALLI MR, AND HOSS W. Regulation of the phosphoinositide cascade by polyamines in brain. *J Neurochem* 63: 1319–1327, 1994.

PETRALIA RS AND WENTHOLD RJ. Light and electron immunocytochemical localization of AMPA-selective glutamate receptors in the rat brain. *J Comp Neurol* 318: 329–354, 1992.

PETRENKO AG. α-Latrotoxin receptor: implications in nerve terminal function. *FEBS Lett* 325: 81–85, 1993.

RAASTAD M, STORM JF, AND ANDERSEN P. Putative single quantum and single fibre excitatory postsynaptic currents show similar amplitude range and variability in rat hippocampal slices. *Eur J Neurosci* 4: 113–117, 1992.

REGEHR WG AND TANK DW. The maintenance of LTP at hippocampal mossy fiber synapses is independent of sustained presynaptic calcium. *Neuron* 7: 451–459, 1991.

REGEHR WG, DELANEY KR, AND TANK DW. The role of presynaptic calcium in short-term enhancement at the hippocmapal mossy fiber synapse. *J Neurosci* 14: 523–537, 1994.

ROSENMUND C AND STEVENS CF. Definition of the readily releasable pool of vesicles at hippocampal synapses. *Neuron* 16: 1197–1207, 1996.

SALIN PA, SCANZIANI M, MALENKA RC, AND NICOLL RA. Distinct short-term plasticity at two excitatory synapses in the hippocampus. *Proc Natl Acad Sci USA* 93: 13304–13309, 1996.

SCANZIANI M, CAPOGNA M, GAHWILER BH, AND THOMPSON SM. Presynaptic inhibition of miniature excitatory synaptic currents by baclofen and adenosine in the hippocampus. *Neuron* 9: 919–927, 1992.

SCHMITZ D, FRERKING M, AND NICOLL RA. Synaptic activation of presynaptic kainate receptors on hippocampal mossy fiber synapses. *Neuron* 27: 327–338, 2000.

SHELTON DP. Membrane resistivity estimated for the purkinje neuron by means of a passive computer model. *Neuroscience* 14: 111–131, 1985.

SIEGEL SJ, JANSSEN WG, TULLAI JW, ROGERS SW, MORAN T, HEINEMANN SF, AND MORRISON JH. Distribution of the excitatory amino acid receptor subunits GluR2(4) in monkey hippocampus and colocalization with subunits GluR5–7 and NMDAR1. *J Neurosci* 15: 2707–2719, 1995.

SPRUSTON N, JONAS P, AND SAKMANN B. Dendritic glutamate receptor channels in rat hippocampal CA3 and CA1 pyramidal neurons. *J Physiol (Lond)* 482: 325–352, 1995.

TURNER DA AND SCHWARTZKROIN PA. Electrical characteristics of dendrites and dendritic spines in intracellularly stained CA3 and dentate hippocampal neurons. *J Neurosci* 3: 2381–2394, 1983.

URBAN NN, HENZE DA, AND BARRIONUEVO G. The hippocampal mossy fiber synapse detonator or discriminator? *Hippocampus* 11: 408–417, 2001.

VOGT KE AND NICOLL RA. Glutamate and gamma-aminobutyric acid mediate a heterosynaptic depression at mossy fiber synapses in the hippocampus. *Proc Natl Acad Sci USA* 96: 1118–1122, 1999.

WASHBURN MS AND DINGLEDINE R. Block of alpha-amino-3-hydroxy-5-methyl-4-isoxazolepropionic acid (ampa) receptors by polyamines and polyamine toxins. *J Pharmacol Exp Therap* 278: 669–678, 1996.

WASSERKORT R, HOPPE E, REDDINGTON M, AND SCHUBERT P. Modulation of A1 adenosine receptor function in rat brain by the polyamine, spermine. *Neurosci Lett* 124: 183–186, 1991.

WEISSKOPF MG AND NICOLL RA. Presynaptic changes during mossy fibre LTP revealed by NMDA receptor-mediated synaptic responses. *Nature* 376: 256–259, 1995.

WILLIAMS SH AND JOHNSTON D. Kinetic properties of two anatomically distinct excitatory synapses in hippocampal CA3 pyramidal neurons. *J Neurophysiol* 66: 1010–1020, 1991.

WYLLIE DJ, MANABE T, AND NICOLL RA. A rise in postsynaptic Ca^{2+} potentiates miniature excitatory postsynaptic currents and AMPA responses in hippocampal neurons. *Neuron* 12: 127–138, 1994.

XIANG Z, GREENWOOD AC, KAIRISS EW, AND BROWN TH. Quantal mechanism of long-term potentiation in hippocampal mossy-fiber synapses. *J Neurophysiol* 71: 2552–2556, 1994.